Journal of Power Sources 243 (2013) 138–146

Contents lists available at SciVerse ScienceDirect

Journal of Power Sources

journal homepage: www.elsevier.com/locate/jpowsour

Effects of nitrogen and carbon monoxide concentrations on performance of proton exchange membrane fuel cells with Pt–Ru anodic catalyst

Chen-Yu Chen [a,*], Wei-Hsiang Lai [a,b], Wei-Mon Yan [c], Chun-Chi Chen [a], Sui-Wei Hsu [d]

[a] Institute of Aeronautics and Astronautics, National Cheng Kung University, No. 1, Ta-Hsueh Road, Tainan 701, Taiwan, ROC
[b] Research Center for Energy Technology and Strategy, National Cheng Kung University, No. 1, Ta-Hsueh Road, Tainan 701, Taiwan, ROC
[c] Department of Greenergy, National University of Tainan, 33, Sec. 2, Shu-Lin St., Tainan 700, Taiwan, ROC
[d] Celxpert Energy Corporation, No. 128, Gong 5th Rd., Longtan Township, Taoyuan County 325, Taiwan, ROC

HIGHLIGHTS

- The dilution effect of N_2 is only significant at low H_2 stoichiometric ratios.
- CO affects PEMFCs in both low current region and high current region.
- Voltage fluctuation of a PEMFC with the Pt–Ru catalyst is observed and discussed.
- Real-time monitoring of the anode outlet CO concentration is performed.
- Fluctuation of the anode outlet CO concentration accompanies voltage fluctuation.

ARTICLE INFO

Article history:
Received 5 March 2013
Received in revised form
8 May 2013
Accepted 2 June 2013
Available online 10 June 2013

Keywords:
Proton exchange membrane fuel cell
Simulated reformate gas
Dilution effect
Poison effect
Voltage fluctuation
Real-time exhaust monitoring

ABSTRACT

The reformate gas is one of the commonest solutions to the problem of fuel supply for proton exchange membrane fuel cell systems. Thus, it is important to understand the behaviors of a fuel cell using reformate gases. In this work, effects of nitrogen and carbon monoxide concentrations on unsteady characteristics of a proton exchange membrane fuel cell with the Pt–Ru anodic catalyst are investigated experimentally. Simulated reformate gases with hydrogen, nitrogen and carbon monoxide are employed as the fuel. The experimental data show that a larger dilution effect of nitrogen is noted for cases with lower hydrogen stoichiometric ratios. Furthermore, increasing the carbon monoxide concentration reduces the cell performance because the elevated carbon monoxide adsorption rate results in a severer poison effect. The voltage fluctuating phenomenon is observed at high CO ppm and is due to a periodical change of coverage on the catalyst surface. Meanwhile, it is verified that the voltage fluctuation is accompanied with a periodical change of the anode outlet carbon monoxide concentration. Furthermore, the fluctuating phenomena of voltage and the anode outlet carbon monoxide concentration are more easily triggered in diluted hydrogen than in non-diluted hydrogen.

1. Introduction

Because of the practice of Kyoto Protocol, many governments have established some policies to reduce the CO_2 emission. One of the most important policies is developing clean and renewable energy technologies, such as wind energy, solar energy, biomass-based energy and hydrogen energy. Fuel cells are regarded as one of the most promising technologies due to their high energy efficiency, low level of noise, zero pollution emission and high system reliability [1]. Fuel multiplicity is as well another reason that fuel cells are feasible because the fuel for fuel cells can be produced from a wide range of fuels, such as nature gas, liquid hydrocarbon fuels, water electrolysis, biomass waste and bio-fuels which are refined from algae, corn, soybean or palm, etc. [2]. A proton exchange membrane fuel cell (PEMFC) is considered a suitable type of fuel cells for mobile applications and small stationary applications, such as ground vehicles, marine vehicles, uninterruptable power supply systems, emergency power supply systems, and residential power generators [3–9]. A typical PEMFC uses pure hydrogen as the anodic fuel and is more suitable for

* Corresponding author. Tel.: +886 62085914; fax: +886 62389940.
E-mail addresses: aeroshower@msn.com, chyuchen@mail.ncku.edu.tw (C.-Y. Chen).

0378-7753/$ – see front matter © 2013 Elsevier B.V. All rights reserved.
http://dx.doi.org/10.1016/j.jpowsour.2013.06.003

mobile applications. However, the storage and the transportation of hydrogen are two major problems of fuel cell systems [9–11]. In those situations, a PEMFC system using hydrogen-rich reformate gas is one of the commonest solutions.

The hydrogen-rich reformate gas can be reformed from various hydrocarbon fuels, including nature gas [12–15], liquefied petroleum gas [16,17], methanol [18–23], ethanol [24–26] and bio-mass fuels [27,28]. Different reforming processes and hydrocarbon fuels result in different reformate gas compositions. The gas composition of the reformate gas varies with the types of reforming method, hydrocarbon sources, catalysts, reactor designs and operational conditions. Among all kinds of reforming method, steaming reforming (SR) and auto-thermal reforming (ATR) are two common reforming processes for a reformate fuel cell system. For an SR reactor using methanol or ethanol as the fuel source, the dry reformate gas usually contains 65–75% H_2, 12–25% CO_2, 3–12% CO and 1–5% CH_4 [18,19,25,26,29,30]. While for an SR reactor using methane or nature gas as the fuel source, the dry reformate gas may consist of 65–70% H_2, 6–20% CO_2, 3–7% CO and 9–20% CH_4 [13,31–33]. The ATR reformate gas from methanol usually comprises 53–57% H_2, 17–20% CO_2, 4–6% CO and 20–30% N_2 [22,23]. Nevertheless, the ATR reformate gas comprises less hydrogen and more residual methane if methanol is replaced by methane [20,21]. The CO and CH_4 concentrations of the reformate gas which is not treated by a clean-up process are too condense for a PEMFC. Thus, residual methane is usually further reformed into hydrogen and carbon dioxide before the reformate gas is supplied to fuel cells. In addition, two further processes, water-gas shift and preferential oxidation (PROX), are usually introduced to reduce the CO concentration. Many previous works have reported that a CO concentration less than 50 ppm [22,23,34–36] can be achieved after the CO removal process with the water-gas shift and PROX reactions. Because air is usually supplied to the reformer for the PROX reaction, the N_2 concentration of the reformate gas from the PROX reaction could be up to 20–50% [22,23]. It is summarized from the previous papers that N_2, CO_2 and CO account for a large proportion of the reformate gas composition in addition to H_2 for most reformate gases which are ready to be supplied to PEMFCs. N_2 and CO_2 may dilute the hydrogen concentration and increase the mass transport resistance of a fuel cell. In addition to the dilution effect, the existence of CO_2 may cause a slight CO poison problem due to the reverse water gas shift reaction (Eq. (1)) [37,38].

$$CO_2 + 2(Pt - H) \leftrightarrow (Pt - CO) + H_2O + Pt \quad (1)$$

Previous literatures [39–44] indicate that CO may poison the Pt/C catalyst on the membrane electrode assembly (MEA), and cause a significant performance drop of a fuel cell, especially when the CO concentration is higher than 10 ppm [45–47]. It is well known that the electrochemical reaction of hydrogen on the Pt catalyst is a two step reaction and follows Eqs. (2) and (3).

$$H_2 + 2Pt \leftrightarrow 2(Pt - H) \quad (2)$$

$$Pt - H \leftrightarrow Pt + H^+ + e^- \quad (3)$$

CO can not only adsorb onto empty Pt sites directly (Eq. (4)), but also on Pt–H sites (Eq. (5)). Additionally, CO binds more strongly to Pt than H_2, and therefore the Pt–CO binding becomes a barrier of Pt–H binding [39].

$$CO + Pt \leftrightarrow Pt - CO \quad (4)$$

$$2CO + 2(Pt - H) \leftrightarrow 2(Pt - CO) + H_2 \quad (5)$$

Many approaches have been devoted to enhance the CO tolerance of the Pt-based catalyst. The major methods include increasing the operating temperature [48–50], introducing the air-bleeding method [47,51–55], and using bimetallic catalysts [56–61]. The operating temperature is limited to the material of the membrane. For nafion-based membrane, the operating temperature is usually under 80 °C. The margin for temperature raise is not much. Thus, introducing the air-bleeding method and using bimetallic catalysts are better solutions to augment the CO tolerance for a nafion-based PEMFC. Using Pt–Ru catalysts to enhance the CO tolerance is popular in a reformate fuel cell system. In this work, the behaviors of a PEMFC with the Pt–Ru catalyst using reformate gases are concentrated and examined in details.

Addition of Ru onto the Pt surface may reduce the Pt–CO bond strength and facilitate CO oxidation. According to the bifunctional mechanism, addition of Ru may accelerate the formation of CO_2 [55,62,63]. The reactions are shown in Eqs. (6) and (7).

$$Ru + H_2O \rightarrow (Ru - OH) + H^+ + e^- \quad (6)$$

$$(Pt - CO) + (Ru - OH) \rightarrow Pt + Ru + CO_2 + H^+ + e^- \quad (7)$$

In the open literatures, many researchers have been devoted to effects of reformate gases on the cell performance. The major objectives of previous studies [40,64–66] were to realize the characteristics of a PEMFC under different gas conditions via the polarization curves tests, cyclic voltammetry tests and electrochemical impedance spectroscopy tests. However, the real-time monitoring of the exhaust gas from the CO poisoned fuel cell was only carried out in one obtainable previous literature [67] so far. Thus, to further understand the behaviors of a PEMFC using reformate gas, the polarization curve and the real-time monitoring of the exhaust gas were performed and presented at different N_2 and CO concentrations in this study.

2. Experimental

2.1. Single fuel cell

In the present study, a self-made single PEMFC with active area of the MEA being 25 cm^2 is used. The end plates and current collection plates were made of aluminum alloy and gold coated copper, respectively. The bipolar plate of graphite was machined with the serpentine type flow field. The silicon based O-ring was used to seal the single cell. The single cell was clipped by ten bolts with a proper assembly torque. The leaking test was performed before the activation to ensure the fuel cell from leaks of hydrogen. The pressure drop was less than 1 psi in 10 min when the stack was filled with nitrogen of 25 psig. The single PEMFC was assembled according to the following procedure: (i) rinsing graphite plates to remove dust and contaminant; (ii) drying graphite plates with a blower; (iii) putting the cathodic end plate, the cathodic current collector, the cathodic gasket, the MEA, the anodic gasket, the anodic current collector and the anodic end plate, in sequence; (iv) tightening ten bolts in a symmetric sequence and increasing the torque by every 10 kg_f-cm until the required torque.

Using the alloy, such as Pt–Mo, Pt–Ti and Pt–Ru as the catalyst [56–58,60,68–70], is one of solutions to CO poisoning, because some alloy catalysts can oxidize CO adsorbed on the catalyst surface. Among all alloys, Pt–Ru is the most common catalyst for commercialized MEAs and in current reformed hydrocarbon fuel cell systems [36,71]. Thus, to connect the previous researches, the effects of reformate gases on behaviors of a PEMFC using the Pt–Ru/C catalyst are examined in details. In the test, the MEA is provided by W. L. Gore & Associates, Inc., and the catalysts for anode and

cathode are the Pt–Ru/C alloy and Pt/C, respectively. The commercial MEA of Gore 5621 is employed. The ratio of Pt loading to Ru loading is 1.0 for the anodic catalyst. The model number of gas diffusion layers is SGL-34BC.

In this work, three MEAs were used. All parameters, including tests using simulated reformate gases, were tested within the guaranteed life for each MEA. Usually, the performance decreases dramatically after an operation under the CO-contained reformate gas due to CO adsorption on the catalyst. A recovery process was adopted to recover the performance before every test. During the recovery process, only pure hydrogen is supplied to the fuel cell for a period of time and the voltage approaches the value in absence of CO. Fig. 1 presents the performance repeatability of one MEA used in this study after the recovery process. It is clear in Fig. 1 that three polarization curves measured under the same conditions within 792 h are almost consistent with each other. Thus, the experimental data are reliable. In this work, the operating cell temperature (T_{cell}), the dew point temperature of the anodic humidifier ($T_{d,a}$) and the dew point temperature of the cathodic humidifier ($T_{d,c}$) were kept at 75 °C, 70 °C and 70 °C, respectively. The flow rate of anodic gas was fixed to be 950 sccm for all cases of the simulated reformate gas. The basic flow rate of air was 200 sccm and the stoichiometric ratio of air was 4.0.

2.2. Experimental setup and facilities

The schematic diagram of the experimental setup is shown in Fig. 2. The voltage, current and power can be measured with this test station, and the data can be acquired through a data acquisition system. The fuel flow rate was monitored by a mass flow controller with LABVIEW software through an analogy to digital converter. The bubbling type humidifier was used in this test station. A heating system was designed to control the dew point temperature of the humidified gas with accuracy being ±1 °C. To supply a simulated reformate gas to the fuel cell, an S-4000 gas mixer (Environics®, USA) was used. The accuracy of the flow rate and the gas concentration is ±1% of the full scale. In this work, the simulated reformate gas was mixed by nitrogen with 99.999% purity, hydrogen with 99.999% purity and 1% CO balanced hydrogen. The real-time CO concentration of the anodic exhaust was measured and recorded by a NGA 2000 multi-component gas analyzer (Rose Analytical Inc., USA).

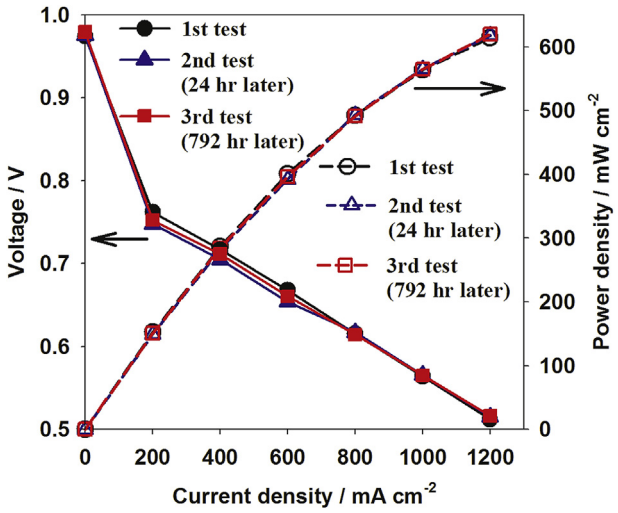

Fig. 1. The performance repeatability of an MEA used in this study (T_{Cell} = 75 °C, $T_{d,a}$ = 70 °C, $T_{d,c}$ = 70 °C).

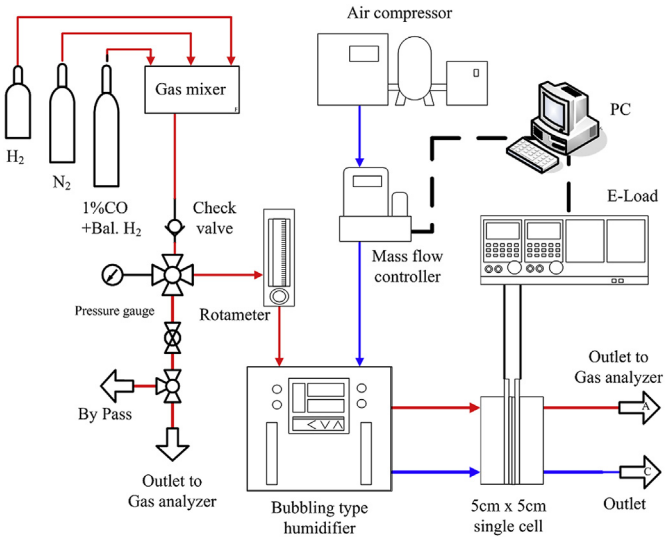

Fig. 2. Schematic diagram of the experimental setup.

3. Results and discussion

3.1. Effects of N_2 concentration in N_2/H_2 mixture

Because N_2 and CO_2 usually account for a large proportion of the reformate gas composition in addition to CO and H_2, fuel cells using the reformate gas may suffer from a negative effect due to diluting hydrogen. Although the presence of CO_2 may cause a slight poison problem, the poison effect caused by CO_2 is negligible compared to that due to CO. Thus, to simplify the experimental process, only N_2 was added into the simulated reformate gas to dilute hydrogen. The effect of the presence of CO_2 was not studied in this part. To understand the effects of different diluted hydrogen levels, the polarization curves of the PEMFC under different gas mixtures of H_2 and N_2 are presented in details. In this part, there is not any CO being mixed in the anodic gas mixture and the flow rate of the anodic gas was fixed at 950 sccm to exclude effects of CO poisoning and hydrogen starvation.

Polarization curves of the fuel cell at various N_2 concentrations are depicted in Fig. 3. An overall inspection of Fig. 3 reveals that the cell performance slightly decreases with increasing the N_2 concentrations when the N_2 concentration is less than 60%. This implies that the presence of N_2 does not cause a serious mass transport polarization if H_2 is still sufficient. A similar phenomenon was reported in Bhatia et al. [72]. However, the cell performance at high loading condition (high current density region) declines significantly for the N_2 concentration being 75%. Hydrogen stoichiometric ratios at 75% N_2 at 800 mA cm^{-2}, 1000 mA cm^{-2} and 1200 mA cm^{-2} are 1.71, 1.37 and 1.14, respectively. Hydrogen stoichiometric ratios at other N_2 concentrations and current densities are all higher than 1.82. Thus, the significant performance drop can be attributed to a relative more significant dilution effect of nitrogen at a lower hydrogen stoichiometric ratio due to a higher resistance of hydrogen diffusion. A similar phenomenon was observed in previous literatures [64,73]. Thus, it can be concluded from Fig. 3 that a larger dilution effect of nitrogen for the fuel cell using N_2/H_2 mixtures is noted for cases with lower hydrogen stoichiometric ratios.

3.2. Effects of CO concentration in CO/H_2 mixture

It is well known that CO poisons the Pt catalyst and reduces the cell performance. In this section, the anode gas mixture is composed

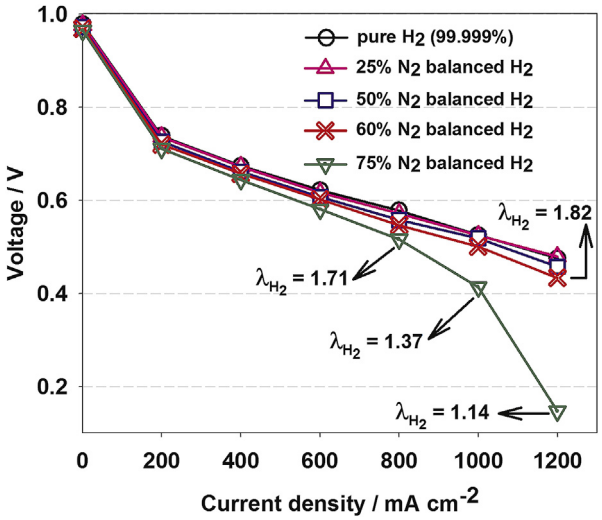

Fig. 3. Polarization curves at different N_2 concentrations in the H_2/N_2 mixture (T_{Cell} = 75 °C, $T_{d,a}$ = 70 °C, $T_{d,c}$ = 70 °C).

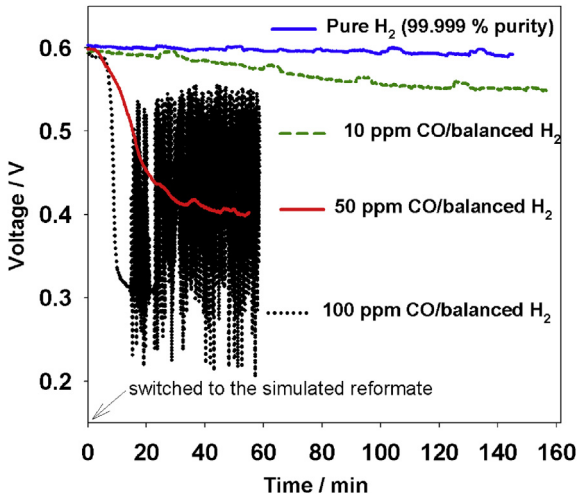

Fig. 5. Transient voltage variations of the fuel cell at different CO concentrations in the CO/H_2 mixture (current density: 600 mA cm^{-2}, T_{Cell} = 75 °C, $T_{d,a}$ = 70 °C, $T_{d,c}$ = 70 °C).

of CO and H_2 only to exclude noise effects due to other gases. Fig. 4 presents the polarization curves of the fuel cell in the CO/H_2 mixture at various CO concentrations. The corresponding voltages at 600 mA cm^{-2} with 0 ppm CO, 10 ppm CO, 50 ppm CO and 100 ppm CO are 0.62 V, 0.58 V, 0.40 V and 0.32 V, respectively. As can be seen, the cell performance declines significantly with increasing the CO concentration. This is due to a higher fraction of Pt coverage by CO gas [74]. Different from the N_2 dilution effect, the CO poison affects the cell performance in both the low and the high current density regions. This is because CO blocks the Pt catalyst, leading to a higher charge transfer resistance at any operational currents. Transient voltage variations of the fuel cell in the CO/H_2 mixture at the current density of 600 mA cm^{-2} for various CO concentrations are shown in Fig. 5. It is clearly found in Fig. 5 that cell voltages remained at 0.6 V before CO/H_2 mixtures of different CO concentrations were fed into the fuel cell. However, cell voltages started to decrease when CO/H_2 mixtures were flowing into the fuel cell. The voltage decreases considerably with increasing the CO concentration. The declined rates in voltage for 0 ppm CO, 10 ppm CO, 50 ppm CO and 100 ppm CO are 0.07 mV min^{-1}, 0.28 mV min^{-1}, 3.55 mV min^{-1} and 20.60 mV min^{-1}, respectively. This can be made plausible from the fact that the CO adsorption rate on the catalyst increases with increasing the CO concentration in the CO/H_2 mixture.

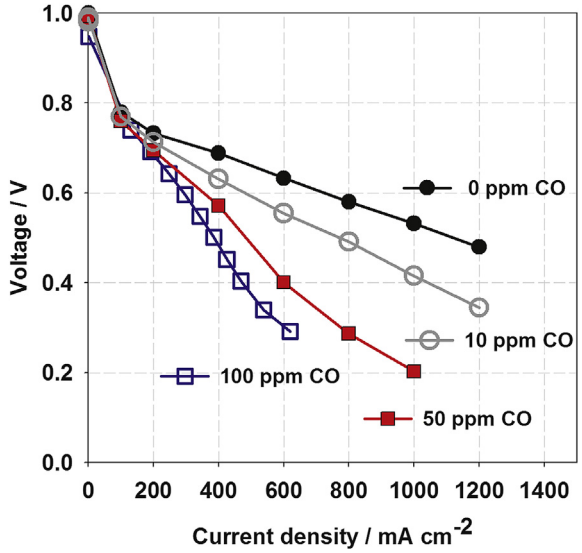

Fig. 4. Polarization curves at different CO concentrations in the CO/H_2 mixture (T_{Cell} = 75 °C, $T_{d,a}$ = 70 °C, $T_{d,c}$ = 70 °C).

In Fig. 5, the voltage for 100 ppm CO will fluctuate at the 15th min. Wagner et al. [75] and Zhang et al. [67,76,77] observed similar phenomena in their works. Wagner et al. mentioned that the Ru catalyst which reactivated the blocked Pt catalyst was regarded as the reason of the voltage fluctuation for a fuel cell using CO-contained fuels. From the electrochemical point of view, the presence of the Ru catalyst would cause the competition between the CO electro-oxidation reaction on the Pt–Ru catalyst and the normal H_2 electro-oxidation reaction on the catalyst surface under galvanostatic operation and lead to a fluctuation of voltage. While from the mechanistical point of view, the Ru catalyst would result in a periodical change of the coverage (change between the fraction of surface coverage by CO, θ_{CO}, and the fraction of surface coverage by H atom, θ_h) of the electrode surface, and therefore cause fluctuation of the voltage [75]. However, the significant voltage fluctuation is only noted for a case with a high CO concentration. Thus, it is concluded that the presence of the Ru catalyst does not necessarily cause a remarkable voltage fluctuation.

In Zhang's study [76], the voltage fluctuation was also attributed to the periodical coverage change of the electrode surface which was affected by the temperature, current density, anode flow rate and the CO concentration. Since the voltage fluctuation is due to the periodical coverage change of the electrode surface, the occurrence of the voltage fluctuation is correlated with rates of gas adsorption, gas desorption and gas oxidation on the catalyst surface. When the adsorption, desorption and electro-oxidation mechanisms of CO and H_2 on the catalyst surface are as the equations listed in Eqs. (8)–(11), the net rates of CO adsorption and H_2 adsorption can be expressed as Eqs. (12)–(14). Moreover, the rates of CO electro-oxidation and H_2 electro-oxidation can be expressed as Eqs. (15) and (16) [72,78,79].

Adsorption and desorption mechanism of CO on the catalyst surface:

$$CO + M \underset{b_{fc}k_{fc}}{\overset{k_{fc}}{\rightleftarrows}} M - CO \quad (8)$$

where M represents a free catalyst site.

Electro-oxidation mechanism of CO on the catalyst surface:

$$H_2O + (M - CO) \overset{k_{ec}}{\rightarrow} M + CO_2 + 2H^+ + e^- \quad (9)$$

Adsorption and desorption mechanism of H_2 on the catalyst surface:

$$H_2 + 2M \underset{b_{fh}k_{fh}}{\overset{k_{fh}}{\rightleftarrows}} 2(M - H) \quad (10)$$

Electro-oxidation mechanism of H_2 on the catalyst surface:

$$M - H \overset{k_{eh}}{\rightarrow} M + H^+ + e^- \quad (11)$$

Net rate of CO adsorption on the catalyst surface:

$$r_{CO,ad} = k_{fc}x_{CO}P\theta_0 - b_{fc}k_{fc}\theta_{CO} \quad (12)$$

Net rate of H_2 adsorption on the catalyst surface:

$$r_{H_2,ad} = k_{fh}x_hP\theta_0 - b_{fh}k_{fh}\theta_h \quad (13)$$

where

$$\theta_0 = 1 - \theta_h - \theta_{CO} \quad (14)$$

Rate of CO electro-oxidation on the catalyst surface:

$$r_{CO} = k_{ec}\theta_{CO}\exp\left[\frac{\eta_a}{RT/\alpha F}\right] \quad (15)$$

Rate of H_2 electro-oxidation on the catalyst surface:

$$r_{H_2} = 2k_{eh}\theta_h\sinh\left[\frac{\eta_a}{RT/\alpha F}\right] \quad (16)$$

For a fuel cell using CO-contained H_2, the total electro-oxidation rate is basically the sum of the H_2 electro-oxidation rate and the CO electro-oxidation rate. Because the total electro-oxidation rate is fixed under the galvanostatic operation, different distributions between the H_2 electro-oxidation rate and the CO electro-oxidation rate on the total electro-oxidation reaction rate cause different overall anode overpotentials. Thus, a periodical change of the electro-oxidation distributions (Eqs. (15) and (16)), which results from a periodic change in the coverage of the electrode, may cause a fluctuation of the anode overpotential for a fuel cell using CO-contained H_2.

The occurrence of a periodical change in the coverage of the electrode can be further explained by the competition between the CO electro-oxidation and the CO adsorption on the catalyst surface. In fact, CO starts to accumulate on the catalyst surface at the beginning of flowing CO-contained H_2 into the fuel cell because the CO oxidation rate is lower than the net CO adsorption rate at this moment. The accumulation of CO on the catalyst leads to a growing fraction of surface coverage by CO. According to Eq. (15), increasing θ_{CO} enhances the CO electro-oxidation rate. Thus, the CO electro-oxidation rate increases while CO is accumulating on the catalyst surface. Otherwise, increasing θ_{CO} decreases the net rate of CO adsorption (Eq. (12)). When the CO electro-oxidation rate is higher than the net CO adsorption rate on the catalyst surface, θ_{CO} starts to reduce, and consequently leads to a declined rate of CO electro-oxidation and an elevated net rate of CO adsorption. As soon as the CO electro-oxidation rate is lower than the net CO adsorption rate on the catalyst surface, θ_{CO} increases again. Therefore, the voltage fluctuates due to the periodical coverage change of the electrode surface and higher voltage fluctuation is noted only for the case with the condenser CO concentration in Fig. 5. Slight or insignificant voltage fluctuation was observed for the CO concentration being 50 ppm or less.

It is inferred that the voltage fluctuation occurs only when the intensity of the competition between the CO adsorption reaction and the CO oxidation reaction reaches a critical point. Increasing the CO concentration of the fed gas raises the maximum fraction of surface coverage by CO, leading to a highly intense competition between the CO adsorption reaction and the CO oxidation reaction. Thus, a significant periodical coverage change of the electrode surface occurs more easily at a high CO concentration. A high fraction of surface coverage by CO is probably the key factor to trigger a remarkable voltage fluctuation in this case. A further study is still needed to clarify the activation mechanism of the voltage fluctuation.

Since the periodical change of the coverage on the catalyst is accompanied with a periodical change of the gas concentration in the PEMFC. Therefore, an oscillation of the CO concentration in the fuel cell is expected to be observed. However, few studies about the oscillation of the CO concentration in the fuel cell were reported in open literatures so far. Thus, to verify the expectation of the oscillation of the CO concentration and to confirm the cause of the voltage fluctuation for a fuel cell with the Pt–Ru catalyst in this work, the real-time monitoring of the CO concentration in the anode exhaust was carried out in the present study. Figs. 6–8 present the transient voltage variations and the transient anode outlet CO concentrations of the fuel cell under a fixed current density of 600 mA cm^{-2} using 10 ppm CO, 50 ppm CO and 100 ppm CO balanced hydrogen, respectively. For conditions of 10 ppm CO and 50 ppm CO balanced hydrogen, the voltage decreases rapidly at the beginning, and reaches a steady value after a period of time. For example, the voltage in Fig. 6 drops rapidly within the first 120 min and approaches a value at about 0.55 V. The real-time monitoring of the anode exhaust reveals that the anode outlet CO concentration does not change significantly during the first 50 min. But, the anode outlet CO concentration increases considerably between the 50th min and the 100th min, and finally reaches a stable value of about 14 ppm. The similar phenomena were also reported in Zhang et al. [67]. It is inferred that the net CO adsorption rate on the catalyst is still positive and higher than the CO oxidation rate within the first 50 min. During this stage, CO accumulates on the catalyst surface rapidly and therefore only little CO remains in the exhaust at the beginning of the test. However, the anode outlet CO concentration increases rapidly after the 50th min. This can be made plausible by noting the fact that the net CO accumulation rate on the catalyst surface starts to reduce, and θ_{CO} is close to the value

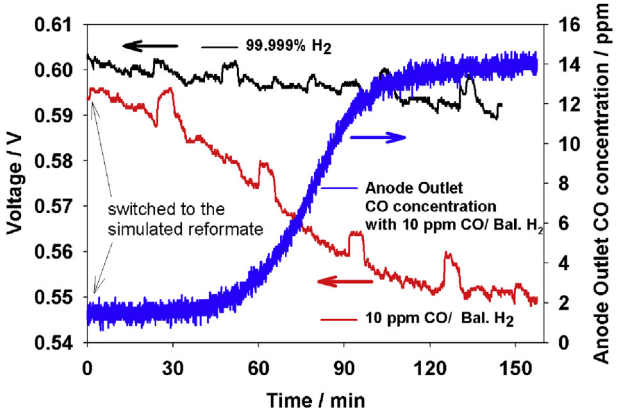

Fig. 6. The transient voltage variation and the transient anode outlet CO concentration of the fuel cell using the 10 ppm CO/H_2 mixture (current density: 600 mA cm^{-2}, T_{Cell} = 75 °C, $T_{d,a}$ = 70 °C, $T_{d,c}$ = 70 °C).

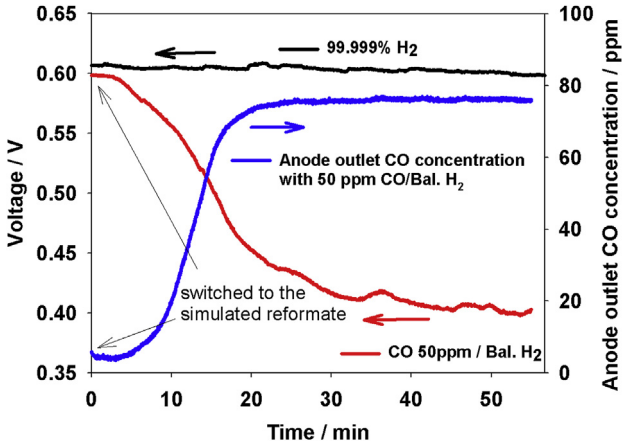

Fig. 7. The transient voltage variation and the transient anode outlet CO concentration of the fuel cell using the 50 ppm CO/H_2 mixture (current density: 600 mA cm^{-2}, T_{Cell} = 75 °C, $T_{d,a}$ = 70 °C, $T_{d,c}$ = 70 °C).

of equilibrium state, leading to an elevated anode outlet CO concentration. After the 100th min, the CO concentration reaches a stable value at about 14 ppm. This is due to the fact that both the CO adsorption and the CO oxidation reach the equilibrium state. Thus, θ_{CO} is in the state of equilibrium as well during this stage. It is noticed that the final stable value of the anode outlet CO concentration is higher than that of the fed gas owing to the balance between consumption of hydrogen due to the electrochemical reaction in the fuel cell and reduction of CO due to the CO electro-oxidation reaction on the catalyst [79].

While the CO concentration of the fed gas is raised to 50 ppm (Fig. 7), the cell voltage drops more quickly than that with 10 ppm CO, and approaches a value at about 0.40 V. This implies that both the CO adsorption and CO oxidation reach an equilibrium state more quickly than those with 10 ppm as well. According to Eq. (12), this feature can be attributed to an increase in the net CO adsorption rate which is caused by an increase in the CO mole fraction. In Fig. 7, the anode outlet CO concentration reaches a stable value at about 75 ppm. Similar to Fig. 6, the anode outlet CO concentration is higher than that of the fed gas. When the CO concentration of the fed gas is further increased to 100 ppm (Fig. 8), the fluctuations in both the cell voltage and the anode outlet CO concentration are noted. The fluctuation phenomenon of the anode outlet CO concentration is coincident with the conclusion that the voltage fluctuation is due to a periodical change of the coverage of the electrode surface. On the other hand, the observed fluctuation of the anode outlet CO concentration verifies the expectation of voltage fluctuation being accompanied with a simultaneous fluctuation of the anode outlet CO concentration, which implies a periodical change of the CO concentration in the fuel cell for a Pt–Ru PEMFC using CO-contained fuels [77]. However, dissimilar to the results of 10 ppm and 50 ppm CO, the anode outlet CO concentration of 100 ppm CO tends to converge at 90 ppm which is lower than that of the fed gas. As it was mentioned earlier in the section, increasing the CO concentration of the fed gas magnified the CO electro-oxidation rate owing to the increase in θ_{CO}. Thus, the observed low anode outlet CO concentration is attributed to a higher reduction rate of CO in the fuel cell due to an accelerated rate of CO electro-oxidation. Zhang et al. [67] concluded that the anode outlet CO concentration was affected by the current density for a Pt–Ru PEMFC using CO/H_2 mixtures as fuels because the rate of CO electro-oxidation changes with the change of the current density. The experimental results in this work are consistent with their conclusions.

3.3. Effects of N_2 concentration in 10 ppm CO/N_2/H_2 mixture

In Section 3.1, effects of the N_2 concentration on the behaviors of the PEMFC in the N_2/H_2 mixture were discussed. To further understand the effects of the N_2 concentration on the PEMFC using the CO-contained fuel, CO/N_2/H_2 mixtures with various N_2 concentrations were used as anodic fuels in this section. The polarization curves of the fuel cell at various N_2 concentrations with the 10 ppm CO/N_2/H_2 mixture are depicted in Fig. 9. It is clearly found that the cell performance declines with increasing the N_2 concentration. Compared to results in Fig. 3, the performance decay is more significant. This indicates that the dilution effect of N_2 becomes more considerable when the anode gas contains CO. It also can be observed that not only the performance in mass transport polarization region, but also those in activation polarization and ohmic polarization regions decrease severely. This is because increasing the N_2 concentration of a CO-contained fuel reduces the net rate of H_2 adsorption on the catalyst, and therefore leads to a relative high net rate of CO adsorption on the catalyst. This inference agrees with results of the transient voltage variations, which are discussed below.

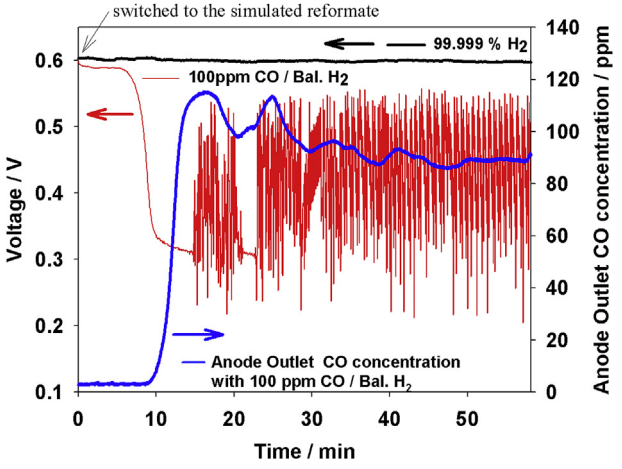

Fig. 8. The transient voltage variation and the transient anode outlet CO concentration of the fuel cell using the 100 ppm CO/H_2 mixture (current density: 600 mA cm^{-2}, T_{Cell} = 75 °C, $T_{d,a}$ = 70 °C, $T_{d,c}$ = 70 °C).

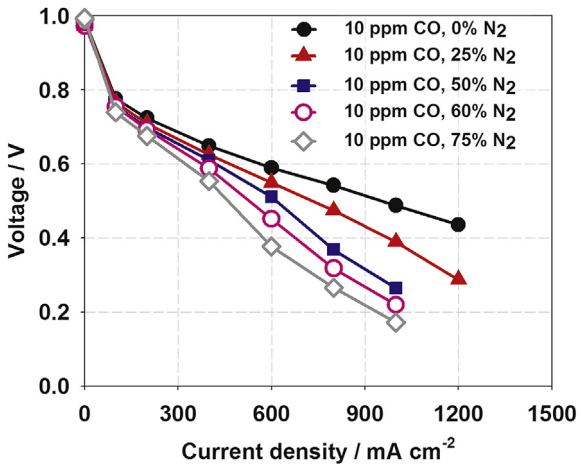

Fig. 9. Polarization curves at different nitrogen concentrations in the 10 ppm CO/N_2/H_2 mixture (T_{Cell} = 75 °C, $T_{d,a}$ = 70 °C, $T_{d,c}$ = 70 °C).

The transient voltage variations at various N_2 concentrations in the 10 ppm CO/N_2/H_2 mixture are shown in Fig. 10. It is clear that cell voltages at 25% N_2, 50% N_2, 60% N_2 and 75% N_2 are stabilized at about 0.54 V, 0.48 V, 0.45 V and 0.36 V, respectively. Both the voltage drop and the descending rate of the voltage increase with the increase in the N_2 concentration. The decay of the stabilized voltage reveals that the fraction of CO coverage on the catalyst increases with increasing the N_2 concentration [74]. On the other hand, the increase of the descending rate of the voltage infers that the net rate of CO adsorption on the catalyst increases with the increase of the N_2 concentration in a CO-contained fuel under galvanostatic operation. Compared to results in Fig. 5, the cell voltage is very stable and there is not any fluctuation. It implies that highly diluted H_2 with a CO concentration of lower than 10 ppm does not cause a remarkable voltage fluctuation.

3.4. Fluctuating phenomena in CO/60% N_2/H_2 mixture

In the previous section, it was concluded the N_2 concentration in the CO-contained reformate gas has a considerable impact on the cell performance of a PEMFC. Previous literatures [71,80] showed that highly diluted hydrogen was used as the anode fuel in some reformate fuel cell systems. Accordingly, to realize the behaviors of the PEMFC with the Pt–Ru catalyst under the highly diluted reformate gas, CO/60% N_2/H_2 mixtures with various CO concentrations were supplied to the fuel cell in this section. Among all characteristics of the PEMFC with Pt–Ru using the reformate gas, voltage fluctuation is a particular phenomenon which is detrimental for the integration of a reliable PEMFC electricity system. Thus, the fluctuating phenomena of the PEMFC in CO/60% N_2/H_2 mixtures are focused in this section. The transient voltage variations at various CO concentrations in the CO/60% N_2/H_2 mixture are indicated in Fig. 11. Similar to Fig. 5, cell voltages in Fig. 11 started to decrease when CO-contained fuels were flowing into the fuel cell. Moreover, both voltage drop and the descending rate of voltage increased with an increase in the CO concentration. However, different from Fig. 5, the voltage fluctuation was observed at CO concentrations of both 50 ppm and 100 ppm. As concluded in Section 3.3, increasing the N_2 concentration of a CO-contained fuel decreases the net rate of H_2 adsorption on the catalyst, and therefore leads to a higher fraction of CO coverage on the catalyst. Thus,

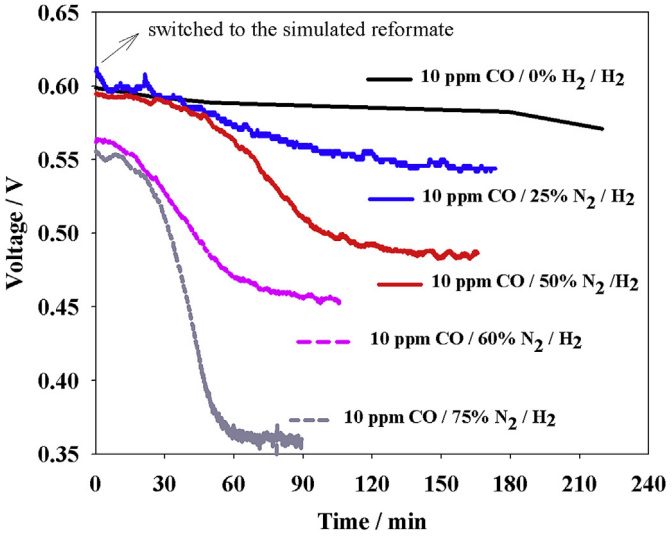

Fig. 10. Transient voltage variations at different nitrogen concentrations in the 10 ppm CO/N_2/H_2 mixture (current density: 600 mA cm^{-2}, T_{Cell} = 75 °C, $T_{d,a}$ = 70 °C, $T_{d,c}$ = 70 °C).

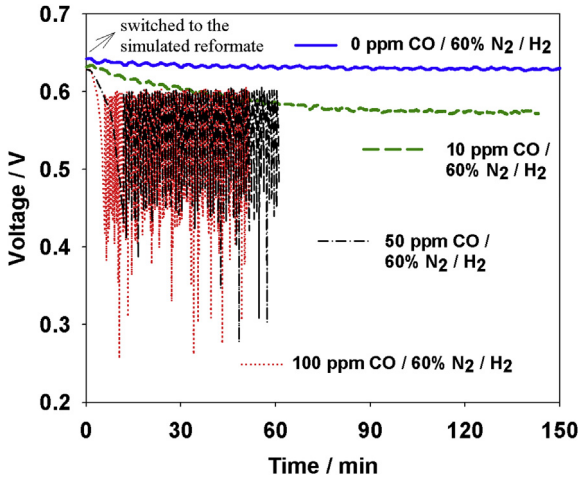

Fig. 11. Transient voltage variations at different CO concentrations in the CO/60% N_2/H_2 mixture (current density: 600 mA cm^{-2}, T_{Cell} = 75 °C, $T_{d,a}$ = 70 °C, $T_{d,c}$ = 70 °C).

the voltage fluctuation is more easily triggered in the diluted hydrogen than in the non-diluted hydrogen.

The transient voltage variations and anode outlet CO concentrations of the fuel cell using the 50 ppm CO/60% N_2/H_2 mixture and the 100 ppm CO/60% N_2/H_2 mixture are disclosed in Fig. 12(a) and

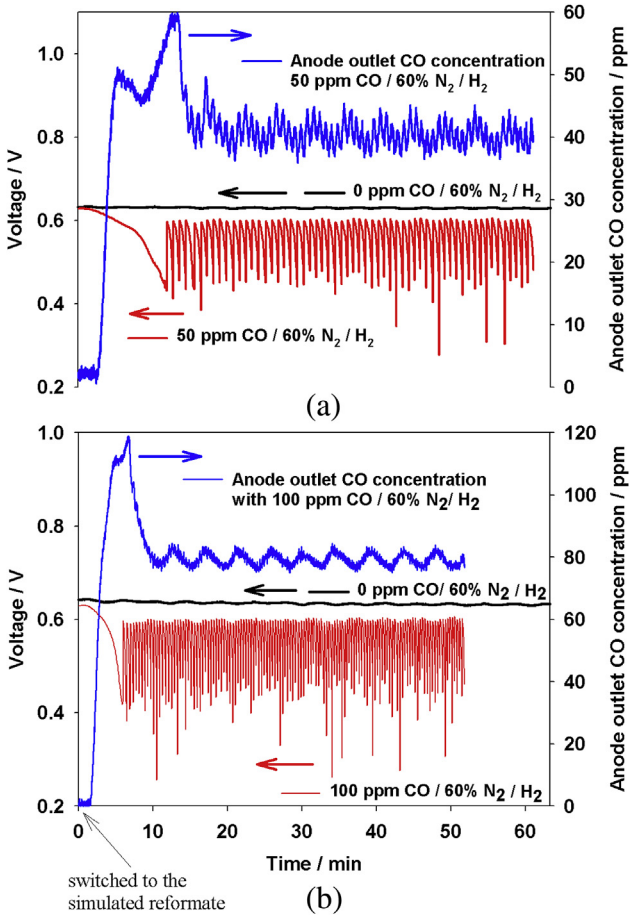

Fig. 12. The transient voltage variation and the transient anode outlet CO concentration of the fuel cell using (a) the 50 ppm CO/60% N_2/H_2 mixture; (b) the 100 ppm CO/60% N_2/H_2 mixture (current density: 600 mA cm^{-2}, T_{Cell} = 75 °C, $T_{d,a}$ = 70 °C, $T_{d,c}$ = 70 °C).

(b), respectively. Overall inspection of Fig. 12 disclosed that the fluctuating phenomena of the voltage and the anode outlet CO concentration started at about the 12th min and 6th min for 50 ppm CO and 100 ppm CO, respectively. Before the occurrence of transient voltage fluctuation, the voltage decreased rapidly and the anode outlet CO concentration increased rapidly as well. In addition, increasing the CO concentration of the fed gas advances the transient voltage fluctuation. It is also observed that the dilution effect of N_2 advances the fluctuation phenomenon (as shown in Figs. 8 and 12(b)). They can be attributed to the accelerated rate of CO accumulation on the catalyst surface, resulting from increasing the CO mole fraction due to the increase in the CO concentration or decreasing the H_2 mole fraction due to the increase in the N_2 concentration. Meanwhile, the anode outlet CO concentration reached a value which was higher than the CO concentration of the fed gas before the fluctuation. However, the anode outlet CO concentration decreased and started to oscillate with an averaged value which was less than that of the fed gas after the fluctuation started. As explained in Figs. 7 and 8, the higher anode outlet CO concentration before the occurrence of fluctuation is due to the balance between the hydrogen consumption and the CO oxidation. Furthermore, after the occurrence of fluctuation in the cell voltage, the low anode outlet CO concentration is due to the elevated rate of the CO electro-oxidation owing to the elevated fraction of the CO coverage.

4. Conclusions

In this work, effects of the N_2 and the CO concentrations of the anode gas on cell performance of a PEMFC with the Pt–Ru catalyst were experimentally studied. The major results are summarized as follows:

1. Increasing the N_2 concentration decreases the cell performance due to the dilution effect. The dilution effect of nitrogen for the fuel cell using N_2/H_2 mixtures is noted for cases with lower hydrogen stoichiometric ratios. Furthermore, increasing the CO concentration decreases the performance as well because the elevated CO adsorption rate results in a significant poison effect.
2. The voltage fluctuation is due to a periodical change of coverage on the catalyst surface. In addition, it is verified that the voltage fluctuation owing to a periodical change of coverage on the catalyst surface is accompanied with a periodical change of the anode outlet CO concentration.
3. The fluctuating phenomena of the voltage and the anode outlet CO concentration are more easily triggered in the diluted hydrogen than in the non-diluted hydrogen.
4. For PEMFCs using the CO-contained fuel, addition of the Ru catalyst improves the tolerance to CO poison. However, to avoid the voltage fluctuation caused by the elevated CO oxidation rate, the CO concentration should be maintained at a lower level, especially for highly diluted H_2.

Acknowledgments

The financial support from National Science Council, ROC, and Celxpert Energy Corporation under grant number NSC 99-2622-E-006-031-CC2 was appreciated. This research was also supported in part by the Headquarters of University Advancement at the National Cheng Kung University, which is sponsored by the Ministry of Education, ROC.

Nomenclature

k_{fc}	rate constant of CO adsorption (A cm^{-2} atm^{-1})
k_{ec}	rate constant of CO electro-oxidation (A cm^{-2})
k_{fh}	rate constant of hydrogen adsorption (A cm^{-2} atm^{-1})
k_{eh}	rate constant of hydrogen electro-oxidation (A cm^{-2})
b_{fc}	backwards forward ratio of CO adsorption (atm)
b_{fh}	backwards forward ratio of hydrogen adsorption (atm)
$r_{CO,ad}$	net rate of CO adsorption on the catalyst surface
r_{CO}	net rate of CO electro-oxidation
$r_{H_2,ad}$	net rate of H_2 adsorption on the catalyst surface
r_{H_2}	net rate of H_2 electro-oxidation
x_{co}	CO mole fraction in the anodic flow channel
x_h	hydrogen mole fraction in the anodic flow channel
P	total pressure (atm)
R	gas constant (8.314 J mol^{-1} K^{-1})
T	fuel cell temperature
F	Faraday's constant (96486 C mol^{-1})
θ_0	fraction of free surface sites
θ_{CO}	fraction of surface coverage by CO
θ_h	fraction of surface coverage by H
η_a	anode overpotential
α	charge transfer coefficient
λ_{H_2}	hydrogen stoichiometric ratio

References

[1] D. Hart, G. Hörmandinger, J. Power Sources 71 (1998) 348–353.
[2] T.E. Lipman, J.L. Edwards, D.M. Kammen, Energy Policy 32 (2004) 101–125.
[3] B. Emonts, J.B. Hansen, H. Schmidt, T. Grube, B. Hohlein, R. Peters, A. Tschauder, J. Power Sources 86 (2000) 228–236.
[4] L. Cardinali, S. Santomassimo, M. Stefanoni, J. Power Sources 106 (2002) 384–387.
[5] H.I. Lee, C.H. Lee, T.Y. Oh, S.G. Choi, I.W. Park, K.K. Baek, J. Power Sources 107 (2002) 110–119.
[6] H.-P. Chang, C.-L. Chou, Y.-S. Chen, T.-I. Hou, B.-J. Weng, Int. J. Hydrogen Energy 32 (2007) 316–322.
[7] P. Beckhaus, M. Dokupil, A. Heinzel, S. Souzani, C. Spitta, J. Power Sources 145 (2005) 639–643.
[8] A. Psoma, G. Sattler, J. Power Sources 106 (2002) 381–383.
[9] I. Staffell, R.J. Green, Int. J. Hydrogen Energy 34 (2009) 5617–5628.
[10] T. Kosugi, A. Hayashi, K. Tokimatsu, Int. J. Hydrogen Energy 29 (2004) 337–346.
[11] M.T. Gencoglu, Z. Ural, Int. J. Hydrogen Energy 34 (2009) 5242–5248.
[12] Y.T. Seo, D.J. Seo, J.H. Jeong, W.L. Yoon, J. Power Sources 163 (2006) 119–124.
[13] E. Jannelli, M. Minutillo, E. Galloni, J. Fuel Cell Sci. Technol. 4 (2007) 435–440.
[14] R.-F. Horng, H.-H. Huang, M.-P. Lai, C.-S. Wen, W.-C. Chiu, Int. J. Hydrogen Energy 33 (2008) 3719–3727.
[15] R.-F. Horng, M.-P. Lai, H.-H. Huang, Y.-P. Chang, Energy Conv. Manag. 50 (2009) 2632–2637.
[16] M. Wichert, Y. Men, M. O'Connell, D. Tiemann, R. Zapf, G. Kolb, S. Butschek, R. Frank, A. Schiegl, Int. J. Hydrogen Energy 36 (2011) 3496–3504.
[17] E. Calò, A. Giannini, G. Monteleone, Int. J. Hydrogen Energy 35 (2010) 9828–9835.
[18] M. Pareta, S.R. Choudhury, B. Somaiah, J. Rangarajan, N. Matre, J. Palande, Int. J. Hydrogen Energy 36 (2011) 14771–14778.
[19] R. Chaubey, S. Sahu, O.O. James, S. Maity, Renew. Sustain. Energy Rev. 23 (2013) 443–462.
[20] V. Palma, A. Ricca, P. Ciambelli, Chem. Eng. J. 207–208 (2012) 577–586.
[21] H.C. Yoon, J.L. Dorr, P.A. Erickson, Int. J. Hydrogen Energy 33 (2008) 2942–2949.
[22] C.-C. Chuang, Y.-H. Chen, J.D. Ward, C.-C. Yu, Y.-C. Liu, C.-H. Lee, Int. J. Hydrogen Energy 33 (2008) 7062–7073.
[23] N. Liu, Z. Yuan, C. Wang, L. Pan, S. Wang, S. Li, D. Li, S. Wang, Chem. Eng. J. 139 (2008) 56–62.
[24] W.-C. Chiu, R.-F. Horng, H.-M. Chou, Int. J. Hydrogen Energy 38 (2013) 2760–2769.
[25] Y.-K. Lee, K.-S. Kim, J.-G. Ahn, I.-H. Son, W.C. Shin, Int. J. Hydrogen Energy 35 (2010) 1147–1151.
[26] J.D. Taylor, C.M. Herdman, B.C. Wu, K. Wally, S.F. Rice, Int. J. Hydrogen Energy 28 (2003) 1171–1178.
[27] T. Aicher, J. Full, A. Schaadt, Int. J. Hydrogen Energy 34 (2009) 8006–8015.
[28] Z.A.B.Z. Alauddin, P. Lahijani, M. Mohammadi, A.R. Mohamed, Renew. Sustain. Energy Rev. 14 (2010) 2852–2862.
[29] V.M. Schmidt, P. Bröckerhoff, B. Höhlein, R. Menzer, U. Stimming, J. Power Sources 49 (1994) 299–313.
[30] Y.-S. Seo, D.-J. Seo, Y.-T. Seo, W.-L. Yoon, J. Power Sources 161 (2006) 1208–1216.
[31] M.D. Falco, G. Iaquaniello, A. Salladini, J. Membr. Sci. 368 (2011) 264–274.

[32] S.-K. Ryi, J.-S. Park, D.-K. Kim, T.-H. Kim, S.-H. Kim, J. Membr. Sci. 339 (2009) 189–194.
[33] M. Levent, D.J. Gunn, M.A. El-Bousiffi, Int. J. Hydrogen Energy 28 (2003) 945–959.
[34] Q. Zhang, L. Shore, R.J. Farrauto, Int. J. Hydrogen Energy 37 (2012) 10874–10880.
[35] C.D. Dudfield, R. Chen, P.L. Adcock, Int. J. Hydrogen Energy 26 (2001) 763–775.
[36] O.J. Kwon, S.-M. Hwang, J.H. Chae, M.S. Kang, J.J. Kim, J. Power Sources 165 (2007) 342–346.
[37] G.J.M. Janssen, J. Power Sources 136 (2004) 45–54.
[38] T. Smolinka, M. Heinen, Y.X. Chen, Z. Jusys, W. Lehnert, R.J. Behm, Electrochim. Acta 50 (2005) 5189–5199.
[39] R.J. Bellows, E.P. Marucchi-Soos, D.T. Buckley, Ind. Eng. Chem. Res. 35 (1996) 1235–1242.
[40] H.S. Chu, C.P. Wang, W.C. Liao, W.M. Yan, J. Power Sources 151 (2006) 1071–1077.
[41] S. Jiménez, J. Soler, R.X. Valenzuela, L. Daza, J. Power Sources 151 (2005) 69–73.
[42] M.S. Wilson, C.R. Derouin, J.A. Valerio, S. Gottesfeld, Los Alamos National Lab, Los Alamos, NM, 1993, Report No.: LA-UR–93-1689.
[43] L.-Y. Sung, B.-J. Hwang, K.-L. Hsueh, F.-H. Tsau, J. Power Sources 195 (2010) 1630–1639.
[44] J. Divisek, H.-F. Oetjen, V. Peinecke, V.M. Schmidt, U. Stimming, Electrochim. Acta 43 (1998) 3811–3815.
[45] J.-H. Wee, K.-Y. Lee, J. Power Sources 157 (2006) 128–135.
[46] H.-F. Oetjen, V.M. Schmidt, U. Stimming, F. Trila, J. Electrochem. Soc. 143 (1996) 3838–3842.
[47] C.-C. Chung, C.-H. Chen, D.-Z. Weng, Appl. Therm. Eng. 29 (2009) 2518–2526.
[48] S.K. Das, A. Reis, K.J. Berry, J. Power Sources 193 (2009) 691–698.
[49] A.R. Korsgaard, R. Refshauge, M.P. Nielsen, M. Bang, S.K. Kaer, J. Power Sources 162 (2006) 239–245.
[50] R. Radu, N. Zuliani, R. Taccani, J. Fuel Cell Sci. Technol. 8 (2011) 051007.
[51] T. Tingelof, L. Hedstrom, N. Holmstrom, P. Alvfors, G. Lindbergh, Int. J. Hydrogen Energy 33 (2008) 2064–2072.
[52] F.A. Uribe, J.A. Valerio, F.H. Garzon, T.A. Zawodzinski, Electrochem. Solid-State Lett. 7 (2004) A376–A379.
[53] W. Shi, M. Hou, Z. Shao, J. Hu, Z. Hou, P. Ming, B. Yi, J. Power Sources 174 (2007) 164–169.
[54] W. Wang, J. Power Sources 191 (2009) 400–406.
[55] A.A. Shah, P.C. Sui, G.-S. Kim, S. Ye, J. Power Sources 166 (2007) 1–21.
[56] D.J. Ham, Y.K. Kim, S.H. Han, J.S. Lee, Catal. Today 132 (2008) 117–122.
[57] C. He, H.R. Kunz, J.M. Fenton, J. Electrochem. Soc. 150 (2003) A1017–A1024.
[58] L.G.S. Pereira, V.A. Paganin, E.A. Ticianelli, Electrochim. Acta 54 (2009) 1992–1998.
[59] S. Mukerjee, R.C. Urian, S.J. Lee, E.A. Ticianelli, J. McBreen, J. Electrochem. Soc. 151 (2004) A1094–A1103.
[60] Y. Kawasoe, S. Tanaka, T. Kuroki, H. Kusaba, K. Ito, Y. Teraoka, K. Sasaki, J. Electrochem. Soc. 154 (2007) B969–B975.
[61] Z. Qi, A. Kaufman, J. Power Sources 113 (2003) 115–123.
[62] L. Giorgi, A. Pozio, C. Bracchini, R. Giorgi, S. Turtu, J. Appl. Electrochem. 31 (2001) 325–334.
[63] F. Maillard, G.-Q. Lu, A. Wieckowski, U. Stimming, J. Phys. Chem. 109 (2005) 16230–16243.
[64] S. Kim, S. Shimpalee, J.W. Van Zee, J. Power Sources 137 (2004) 43–52.
[65] J.-D. Kim, Y.-I. Park, K. Kobayashi, M. Nagai, J. Power Sources 103 (2001) 127–133.
[66] W.A. Adams, J. Blair, K.R. Bullock, C.L. Gardner, J. Power Sources 145 (2005) 55–61.
[67] J. Zhang, R. Datta, Electrochem. Solid-State Lett. 6 (2003) A5–A8.
[68] B.N. Grgur, N.M. Markovic, P.N. Ross, J. Electrochem. Soc. 146 (1999) 1613–1619.
[69] D.A. Stevens, J.M. Rouleau, R.E. Mar, R.T. Atanasoski, A.K. Schmoeckel, M.K. Debe, J.R. Dahn, J. Electrochem. Soc. 154 (2007) B1211–B1219.
[70] T. Ioroi, K. Yasuda, Z. Siroma, N. Fujiwara, Y. Miyazaki, J. Electrochem. Soc. 150 (2003) A1225–A1230.
[71] X. Yan, S. Wang, X. Li, M. Hou, Z. Yuan, D. Li, L. Pan, C. Zhang, J. Liu, P. Ming, B. Yi, J. Power Sources 162 (2006) 1265–1269.
[72] K.K. Bhatia, C.-Y. Wang, Electrochim. Acta 49 (2004) 2333–2341.
[73] L. Hedström, T. Tingelöf, P. Alvfors, G. Lindbergh, Int. J. Hydrogen Energy 34 (2009) 1508–1514.
[74] C.-P. Wang, H.-S. Chu, J. Power Sources 159 (2006) 1025–1033.
[75] N. Wagner, M. Schulze, Electrochim. Acta 48 (2003) 3899–3907.
[76] J. Zhang, R. Datta, J. Electrochem. Soc. 149 (2002) A1423–A1431.
[77] J. Zhang, R. Datta, J. Electrochem. Soc. 151 (2004) A689–A697.
[78] T.E. Springer, T. Rockward, T.A. Zawodzinski, S. Gottesfeld, J. Electrochem. Soc. 148 (2001) A11–A23.
[79] J. Zhang, T. Thampan, R. Datta, J. Electrochem. Soc. 149 (2002) A765–A772.
[80] H.-S. Chu, F. Tsau, Y.-Y. Yan, K.-L. Hsueh, F.-L. Chen, J. Power Sources 176 (2008) 499–514.